nature cell biology

LETTERS

The cell junction protein VAB-9 regulates adhesion and epidermal morphology in *C. elegans*

Jeffrey S. Simske[1,4,5], Mathias Köppen[1,3], Paul Sims[1], Jonathan Hodgkin[2], Alicia Yonkof[4] and Jeff Hardin[1]

Epithelial cell junctions are essential for cell polarity, adhesion and morphogenesis. We have analysed VAB-9, a cell junction protein in *Caenorhabditis elegans.* VAB-9 is a predicted four-pass integral membrane protein that has greatest similarity to BCMP1 (brain cell membrane protein 1, a member of the PMP22/EMP/Claudin family of cell junction proteins) and localizes to the adherens junction domain of *C. elegans* apical junctions[1–4]. Here, we show that VAB-9 requires HMR-1/cadherin for localization to the cell membrane, and both HMP-1/α-catenin and HMP-2/β-catenin for maintaining its distribution at the cell junction. In *vab-9* mutants, morphological defects correlate with disorganization of F-actin at the adherens junction; however, localization of the cadherin–catenin complex and epithelial polarity is normal. These results suggest that VAB-9 regulates interactions between the cytoskeleton and the adherens junction downstream of or parallel to α-catenin and/or β-catenin. Mutations in *vab-9* enhance adhesion defects through functional loss of the cell junction genes apical junction molecule 1 (*ajm-1*) and discs large 1 (*dlg-1*), suggesting that VAB-9 is involved in cell adhesion. Thus, VAB-9 represents the first characterized tetraspan adherens junction protein in *C. elegans* and defines a new family of such proteins in higher eukaryotes.

Polarity is an essential feature of epithelia, which are characterized by functionally distinct apical and basolateral surfaces separated by continuous circumferential cellular junctions[5]. Adherens junctions mediate cell adhesion and tissue morphogenesis, whereas the more apical vertebrate tight junction regulates cell polarity and paracellular trafficking between cells and cell layers[6]. The apical epidermal cell junction in *C. elegans* has just a single discernable electron-dense structure, but nevertheless contains distinct domains (Fig. 1a). The adherens junction regulates epithelial adhesion during ventral enclosure and contains the proteins HMR-1/cadherin, HMP-1/α-catenin and HMP-2/β-catenin[7,8]. A second region basal to the adherens junction, defined by DLG-1 (a MAGUK family cell junction protein) and AJM-1 (a coiled-coil-domain protein) localization, is required for epithelial tightness and is thought to regulate paracellular permeability[9–13]. The region apical to the adherens junction in *C. elegans* intestinal epithelia and the *Drosophila* SAR (subapical region) share molecular similarities with the vertebrate tight junction, as conserved junctional protein complexes, such as the PAR protein complex (which regulates tight junction assembly in vertebrates and epithelial cell polarity in *Drosophila*) are localized at this apical region[14]. In *Drosophila* epithelia, a third distinct apical junction, the septate junction, is localized basal to the adherens junction and regulates epithelial barrier functions[15,16]. The identification of novel cell junction proteins will be essential for discovering how junctional dynamics direct tissue morphogenesis. In this study, we provide an initial characterization of the cell junction protein VAB-9.

vab-9 animals have no cell lineage defects but egg-laying, body morphology and tail morphology defects are variably detected. *vab-9* animals frequently have severe body shape defects in the first larval stage, including dorsal humps (Fig. 1c). To determine whether shape defects result from uneven elongation along the length of *vab-9* animals, we visualized the cell borders of the lateral epidermal (seam) cells *in vivo* using AJM-1–green fluorescent protein (GFP), a fusion protein that localizes to epithelial cell junctions (Fig. 1b)[13,17]. We found that elongation defects correlate with regions in which seam cells fail to undergo proper anteroposterior elongation (Fig. 1c, d). Two observations suggested that elongation in *vab-9* animals is abnormal, but not completely defective. First, elongation progresses normally in at least some cells of *vab-9* animals (compare the elongation of seam cells H2 and V6 in Fig. 1d) and the particular regions that are elongation defective vary between animals. Second, *vab-9* animals with severe body shape defects in the first larval stage ultimately elongate sufficiently to develop into fertile adults (data not shown).

Elongation of the embryo depends on the coordinated contraction of circumferential F-actin[18]. Filaments are localized in the apical region of epidermal cells and mechanically link cells through attachments at adherens junctions[7]. To determine whether the organization of circumferential actin filaments is abnormal in *vab-9* animals, we stained *vab-9* mutants with Alexa–phalloidin. In *vab-9* animals, two principal defects were observed. First, in the most severely affected embryos, bands of circumferential filaments were clustered between regions with reduced numbers of filaments (Fig. 1e). We were unable to determine whether the total number of filaments was reduced, rather than redistributed, in *vab-9* animals. Second, some filaments failed to insert into the adherens junction and often clustered inappropriately

[1]Department of Zoology, University of Wisconsin, Madison, 1117 West Johnson Street, Madison, WI 53706 USA. [2]Genetics Unit/Department of Biochemistry, University of Oxford, South Parks Road Oxford, OX1 3QU, UK. [3]Current Address: Max Planck Institute of Molecular Cell Biology & Genetics, Pfotenhauerstrasse 108, Rm. 435 01307, Dresden, Germany. [4]Rammelkamp Center for Education and Research 2500 MetroHealth Drive Cleveland, OH 44109-1998, USA. [5]Correspondence should be addressed to J.S.S. (e-mail: jsimske@metrohealth.org).

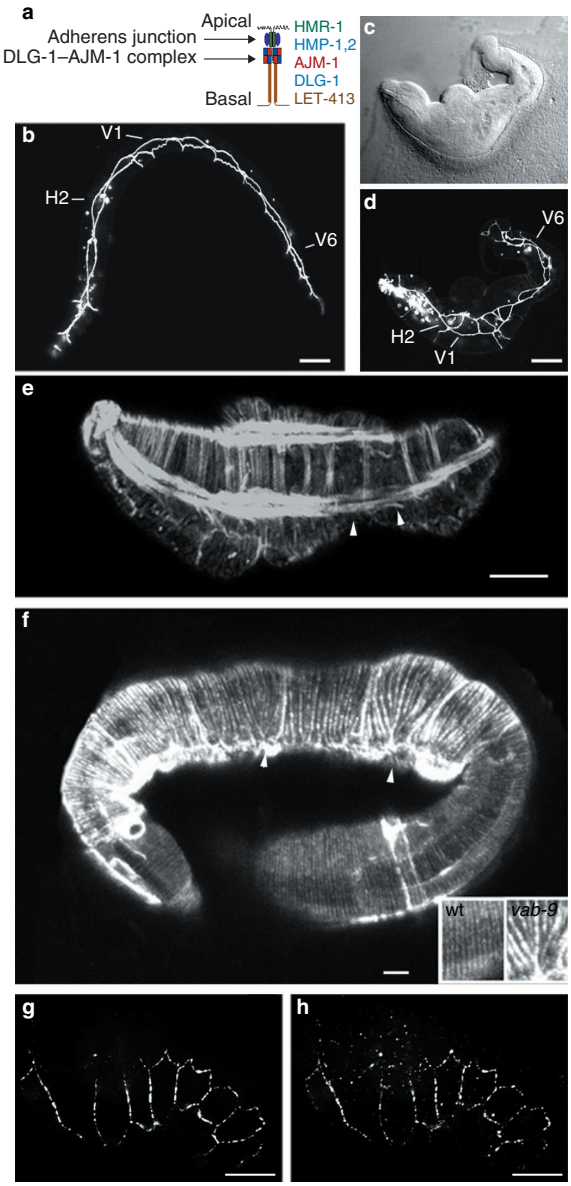

Figure 1 *vab-9* epidermal phenotypes. (**a**) Schematic representation, showing the localization of cell junction proteins in the *C. elegans* epidermis (hypodermis). (**b**, **d**) Determination of seam cell shape through AJM-1–GFP localization, which outlines the apical periphery of epithelial cells in a wild-type L1 larvae, as shown in **b**, and in a *vab-9* mutant, as shown in **d**. In *vab-9* animals, successful elongation is observed in some seam cells (for example, V6), but not in others (for example, H2 and V1). (**c**) Matching DIC image of the *vab-9* mutant in **d**, showing body and tail morphology defects. (**e**, **f**) The organization of circumferential F-actin filaments in *vab-9* animals, as determined by phalloidin staining. In L1 *vab-9* larvae, as shown in **e**, the number of circumferential filaments is reduced and gaps are evident (arrowheads). In older larvae, as shown in **f**, weak body shape defects are associated with regions where circumferential actin filaments cluster abnormally and fail to attach at adherens junctions (arrowheads). Inset shows that filaments are evenly spaced in wild-type larvae (left) and clustered in *vab-9* larvae (right). (**g**, **h**) Mutations in *vab-9* do not affect the junctional localization of HMP-1, as shown in **g**, or HMR-1, as shown in **h**. Scale bar represents 10 μm in all panels.

(Fig. 1f). Regions with defects in filament attachment seem to correlate with body shape defects. The attachment of circumferential actin filaments to adherens junctions in the dorsal hypodermis require adherens junction components (for example, HMP-1/α-catenin)[7]. One simple hypothesis for the defects in circumferential actin organization observed in *vab-9* animals is that HMR-1 or HMP-1 fail to localize at the adherens junction. We tested this possibility by examining the localization of HMP-1 and HMR-1 in *vab-9* animals and found that both were localized correctly (Fig. 1g, h). These results suggest that defects in the distribution of circumferential F-actin in *vab-9* mutants do not result simply from mislocalization of HMP-1 or HMR-1.

We cloned *vab-9* using standard techniques and identified lesions in the *vab-9* alleles *e1744* (W166-STOP), *e2016* (a 100-bp deletion spanning the second intron–third exon boundary) and *ju6* (a 100-bp deletion spanning the third intron–fourth exon boundary; see Fig. 2a and methods). These mutations reduced or eliminated VAB-9 protein levels (Fig. 2f, m). *vab-9* is predicted to encode a 211-amino-acid protein that is conserved from worms to humans and is most similar to a subgroup of the PMP-22/EMP/Claudin family, which includes canine BCMP1 and a *Drosophila* EST (*CG6982*). VAB-9 has four predicted transmembrane helices and a membrane-spanning topology similar to that of PMP22/EMP/Claudin family proteins (Fig. 2b). Members of the PMP-22/EMP/Claudin family of proteins localize to regions of cell–cell adhesion in epithelia, and claudins 1 and 2 were originally identified as major protein components of tight junction strands[1,2,4,19,20].

The subcellular localization of VAB-9 was determined by using an antibody raised against the C terminus of VAB-9 and through expression of a rescuing VAB-9–GFP fusion protein. Both techniques gave essentially the same results. VAB-9 was expressed at the apical region of the lateral membrane region in all epithelia, including hypodermis, pharynx, intestine, vulva, uterus, spermatheca and hindgut (Fig. 2c,d, h and j). VAB-9–GFP was also expressed in the nerve ring (data not shown). VAB-9 expression was undetectable when epithelia initially form, was weakly expressed in dorsal and ventral hypodermis, and ultimately was more strongly expressed in the lateral (seam) hypodermis during elongation (Fig. 2k, l and data not shown). VAB-9 antibodies are most probably specific, as they recognized an epitope *in situ* and a protein on western blots that is missing in all *vab-9* alleles tested (Fig. 2f and m, respectively). VAB-9 has no obvious role in cell polarity, as the localization of apical AJM-1, basolateral LET-413–GFP and intermediate filament proteins required for attachment of muscle to the basal membrane of the epidermis appear normal in *vab-9* animals (Fig. 2g, n–q)[10,21,22].

Next, we determined to which junctional complex VAB-9 localizes. In *C. elegans,* the lateral membranes of epidermal epithelia are very short, making it difficult to distinguish separate localization domains by immunostaining. To address this problem, we stained tetraploid embryos, which are often twice as large as wild-type embryos[23]. HMR-1 was localized apical to AJM-1 (Fig. 3 a–c), which we confirmed by rotating stacked sections through 90° and projecting the lateral membrane (Fig. 3d). VAB-9 also localized apical to AJM-1 in the lateral membrane (Fig. 3e–h). In contrast, VAB-9 and HMP-1 showed precise colocalization (Fig. 3i–l). These results confirm that VAB-9 localizes to the same domain along the apicobasal axis as the cadherin–catenin complex and reinforce previous data indicating that there are distinct sub-domains in the apical junction[9,11–13].

We then tested the requirement of adherens junction components for localization of VAB-9. *hmr-1* is required for junctional localization of VAB-9, as no VAB-9 junctional localization was observed in animals treated with *hmr-1* RNAi, whereas AJM-1 localized normally (Fig. 4 a–c). In *hmp-1* mutants, however, VAB-9 localized to the adherens junction, whereas the distribution of VAB-9 about the periphery of the

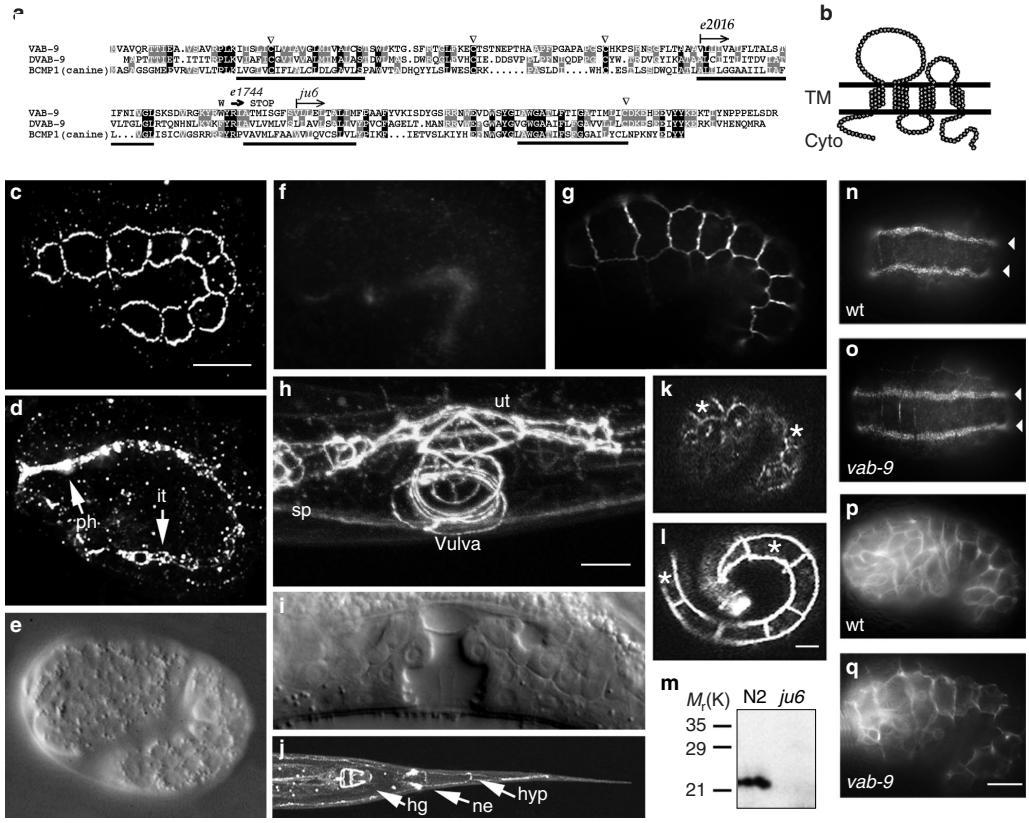

Figure 2 Molecular analysis and expression of VAB-9. (**a**) Comparison of the VAB-9 amino-acid sequence with canine BCMP1 and a predicted protein from *Drosophila* (DVAB-9). Predicted transmembrane domains are underlined. Carats indicate conserved cysteines in PMP22/EMP/Claudin family proteins. Regions of VAB-9 deleted in *e2016* and *ju6* and the *e1744* premature stop are indicated above the alignment. (**b**) Predicted VAB-9 membrane topology in the cell membrane. The Kyte and Doolittle hydrophobicity algorithm predicts similar transmembrane regions (data not shown). TM, transmembrane region; cyto, cytoplasmic region. VAB-9 is expressed in all epithelia, as revealed by staining with VAB-9 antibodies (**c** and **d**) or by VAB-9–GFP fluorescence (**h**, **j**, **k** and **l**). (**c**, **d**) VAB-9 is localized to epithelial cell junctions in seam cells, as shown in **c**, and pharynx (ph) and intestine (it), as shown in **d**. (**f**, **g**) VAB-9 is not detected in *vab-9 (ju6)* animals, as shown in **f**, but AJM-1 localizes correctly, as shown in **g**. (**h**) Postembryonic VAB-9–GFP expression is shown in vulva, uterus (ut) and spermatheca (sp). (**j**) In the posterior, VAB-9–GFP is expressed in hindgut (hg), tail epidermal cells hyp8–hyp11 (hyp) and in phasmids (ne). (**e**, **i**) DIC (Nomarski) images of a comma-stage embryo, as shown in **e**, and a fourth-larval-stage animal, as shown in **i**, of the same developmental stage as animals in **c** and **h**, respectively. (**k**, **l**) VAB-9–GFP expression at comma and threefold stages, respectively. Asterisks indicate equivalent seam cells. (**m**) Western blot of whole-worm extracts from wild-type (N2) and *vab-9 (ju6)* animals using anti-VAB-9 antibodies. A specific band of approximately the expected size is found in wild type, but is absent from *vab-9 (ju6)* mutants. (**n**, **o**) MH4 staining in wild-type and *vab-9* animals respectively. Localization of the MH4 epitope in dorsal quadrants is indicated with arrowheads (the MH27 antibody was included in this experiment and faintly stains AJM-1 at junctions). (**p**, **q**) Expression of LET-413–GFP in wild-type, as shown in **p**, and *vab-9* embryos, as shown in **q**. In each case, anterior is to the left, and dorsal is up, except in **j**, which is viewed from the ventral side. Scale bar represents 10 μm.

junction was punctate and discontinuous (Fig. 4d). Interestingly, the HMR-1 localization pattern in animals treated with *hmp-1* or *hmp-2* RNAi was very similar to that of VAB-9 (Fig. 4e, f and data not shown). To determine whether mislocalization of VAB-9 in *hmp-1* embryos resulted from loss of initial, normally localized VAB-9, or from a failure in distribution about the periphery of the junction, VAB-9–GFP localization was monitored throughout development in *hmp-1* RNAi-treated animals using multiphoton laser-scanning microscopy (MPLSM)[24]. In wild-type, *hmp-1 or hmp-2* RNAi-treated embryos, VAB-9–GFP was initially distributed about the periphery of the adherens junctions, but was then rapidly mislocalized in *hmp-1 or hmp-2* RNAi-treated embryos (Fig. 4g, h and data not shown). Such rapid mislocalization of VAB-9–GFP indicates that the lateral movement of VAB-9 within the membrane of the junctional domain is less restricted in epithelial cells of *hmp-1* RNAi-treated embryos than in wild-type embryos. Using MPLSM, we also found that in *hmr-1* RNAi-treated embryos, VAB-9–GFP never localized to cell junctions (data not shown). These results indicate that HMR-1 is required for localization of VAB-9 to cell junctions and that HMP-1 and HMP-2 are required to maintain the distribution of both VAB-9 and HMR-1 around the periphery of the adherens junction.

As previous studies have demonstrated that components of the adherens junction are not required for localization of AJM-1 and that the DLG-1–AJM-1 complex is not required for localization of HMP-1 (refs 7, 9, 11–13), we tested whether VAB-9 localization requires *ajm-1* or *dlg-1*. When *ajm-1, dlg-1* or both were inactivated, VAB-9 (and HMP-1) localization was unaffected (Fig. 5a, b). Conversely, the localization of AJM-1 and DLG-1 in *vab-9* mutants was normal (Figs 1d, 2g and data not shown). Similarly, double-mutant combinations between adherens junction genes (for example, *vab-9*; *hmp-1* RNAi or *vab-9*; *hmr-1* RNAi) had no effect on AJM-1 localization (data not shown). In general, these results suggest that protein localization to these distinct

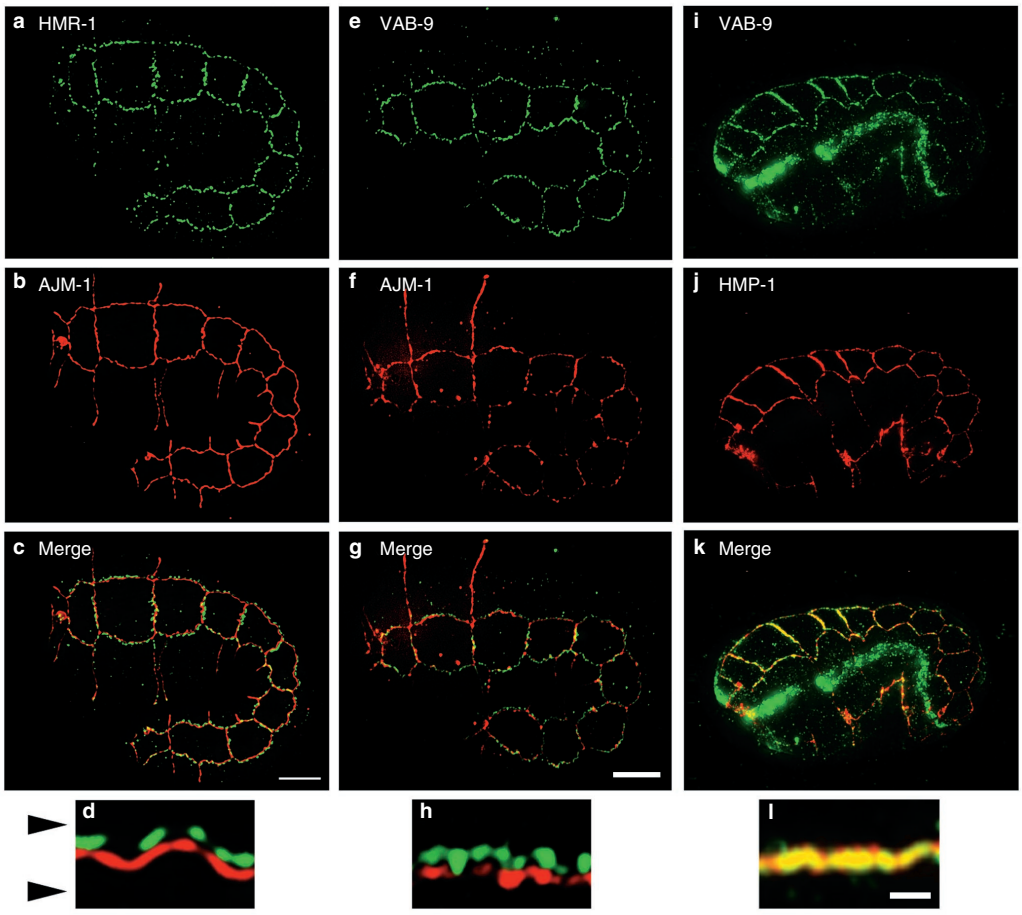

Figure 3 VAB-9 colocalizes with adherens junction components. Images of SP346 twofold (**a**–**h**) and comma-stage (**i**–**l**) embryos costained for HMR-1 and AJM-1 (**a**–**d**), VAB-9 and AJM-1 (**e**–**h**), and VAB-9 and HMP-1 (**i**–**l**). HMR-1 (**a**), VAB-9 (**e**, **i**) and HMP-1 (**j**) are expressed at the cellular junctions of lateral seam cells in a pattern similar to that of AJM-1 expression (**b**, **f**). Merged images of the deconvolved, projected images through 6.8 μm of the lateral surface are shown (**c**, **g** and **k**). (**d**, **h** and **l**) Projections of seam-dorsal cell membranes along the apicobasal axis were generated through a 90° rotation of the stack of lateral images. HMR-1 (**d**, green) and VAB-9 (**h**, green) are apical to AJM-1 (red), and VAB-9 colocalizes with HMP-1 (**l**, yellow). The apical and basal limits of the cell are indicated with arrowheads and were determined by costaining with βG-spectrin, which localizes to the basolateral surface of epithelia[31] (data not shown). Scale bar represents 10 μm for all panels, except **d**, **h** and **l** where scale bar represents 1 μm.

junctional regions is mutually independent. Consistently, the localization of VAB-9/HMP-1 and AJM-1 were qualitatively distinct in *let-413* embryos (see Supplementary Information, Fig. S1).

As VAB-9 and AJM-1/DLG-1 localize independently and have distinct and separable functions on the basis of phenotype, we examined the phenotypes of *vab-9* and *ajm-1* single mutants, or *vab-9; dlg-1* and *vab-9; ajm-1* double mutants. *ajm-1* and *dlg-1* animals arrested at either the twofold or threefold stage of elongation, but did not rupture (Fig. 5d)[9,11–13], whereas *vab-9* embryos enclosed and developed into fertile adults despite irregular elongation and body shape defects. In contrast, 52% ($n = 92$) of *vab-9; ajm-1* and 69% ($n = 26$) of *vab-9; dlg-1* RNAi-treated animals (Fig. 5e) arrested earlier in development than *ajm-1* or *dlg-1* alone (that is, before the twofold stage) with rupturing of the epidermis. These results suggest that *vab-9* and *ajm-1/dlg-1* mediate partially redundant adhesive functions in the epidermis. To determine more precisely the nature of the *vab-9; ajm-1* adhesive defects, we obtained transmission electron microscopy (TEM) images of cellular junctions in these animals (Fig. 5f–i). We scored individual cell–cell contacts as wild type (Fig. 5f; normal, with a single apical electron-dense region at the junction and closely apposed cell membranes along the apicobasal axis), *ajm-1*-like (Fig. 5h; with discrete bubble-like separations between adjacent cell membranes within the electron-dense material of the cell junction)[13], or severe (Fig. 5i; separated by large gaps that may extend along the entire length of the apicobasal axis). Of 150 junctions scored in 8 wild-type embryos, 144 were normal, 6 were *ajm-1*-like and none were severe. Of 69 junctions in 7 *vab-9* embryos, 65 were normal and 4 were *ajm-1*-like (Fig. 5 g). Of 46 junctions in 4 *ajm-1* mutants, 10 were normal, 33 were *ajm-1*-like and 3 were severe (Fig. 5h). In contrast, of the 101 epidermal junctions from 9 *vab-9; ajm-1* embryos examined, 22 were normal, 18 were *ajm-1*-like and 61 were severe. Thirty-five of these severe separations involved gaps ranging from 10–100 nm, whereas 26 involved complete separations of the lateral membranes of opposed cells (Fig. 5j). A complete separation of lateral membranes was never observed in *vab-9* or *ajm-1* single-mutant embryos. Thus, the cell adhesion defects observed by TEM in *vab-9; ajm-1* embryos are more severe than the adhesion defects in either single mutant.

To test whether *vab-9* activity depends on adherens junction genes and whether VAB-9 is a downstream target of these genes, we characterized the genetic interactions between *vab-9* and *hmr-1, hmp-1* and

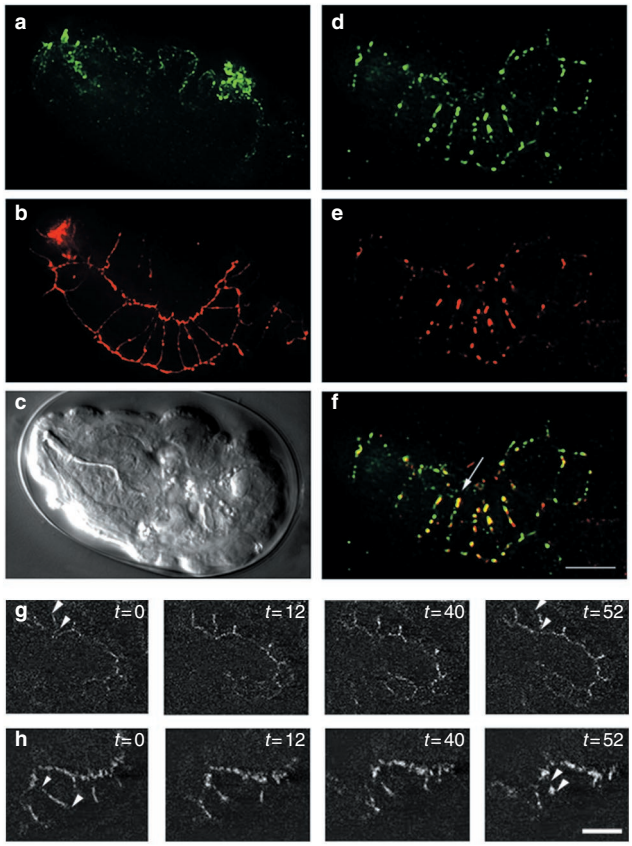

Figure 4 VAB-9 localization requires HMR-1, HMP-1 and HMP-2. (**a–c**) *hmr-1* RNAi-treated animal stained with VAB-9 antibodies, as shown in **a**, and AJM-1 antibodies, as shown in **b**. A DIC image of an equivalently staged *hmr-1* embryo with a humpback (Hmp) phenotype is shown in **c**. (**d–f**) *hmp-1* RNAi-treated animals stained with VAB-9 antibodies, as shown in **d** and HMR-1 antibodies, as shown in **e**. The merged image of **d** and **e** is shown in **f**. VAB-9 and HMR-1 are similarly mislocalized in *hmp-1* RNAi-treated animals and regions of colocalization are shown in yellow (arrow). Scale bar represents 10 μm. (**g**, **h**) Selected panels from multiphoton time-lapse recordings of VAB-9–GFP in wild-type animals, as shown in **g**, and *hmp-1* RNAi-treated animals, as shown in **h**. The initial distribution of VAB-9–GFP about the peripheral apical axis of epidermal cells persists in wild-type animals, but not *hmp-1* RNAi-treated animals. Arrowheads highlight selected regions of junctional VAB-9–GFP expression. Time is shown in minutes. Scale bar represents 10 μm.

hmp-2. Loss of maternal and zygotic *hmr-1*, *hmp-1* and *hmp-2* activity results in partial or complete enclosure defects in 89% ($n = 186$), 82% ($n = 44$) and 81% ($n = 67$) of animals, respectively[8]. In a *vab-9* mutant background, enclosure defects occur in 95% ($n = 40$), 74% ($n = 46$) and 69% ($n = 35$) of *hmr-1*, *hmp-1* and *hmp-2* animals, respectively. Thus, mutations in *vab-9* do not enhance strong loss-of-function *hmr-1*, *hmp-1* or *hmp-2* phenotypes. To generate partial loss-of-function *hmp-1* or *hmp-2* phenotypes, we soaked worms in double-stranded RNA (although we were unable to induce weak RNAi effects using the soaking method in the case of *hmr-1*). Under these conditions, we observed that 19% ($n = 60$) and 23% ($n = 112$) of *hmp-1* and *hmp-2* RNAi-treated animals, respectively, were enclosure defective. However, in a *vab-9* mutant background, 52% ($n = 37$) and 48% ($n = 27$) of animals treated with *hmp-1* or *hmp-2* dsRNA, respectively, were enclosure defective, demonstrating that *vab-9* enhances weak *hmp-1* and *hmp-2* RNAi phenotypes. Finally, we observed that all of the rare *hmp-1* ($n = 15$) and *hmp-2* ($n = 10$) RNAi larvae generated by soaking in dsRNA displayed phenotypes similar to *vab-9* body shape defects (data not shown). These genetic results suggest that *vab-9* functions in the adherens junction pathway, but do not order *vab-9* function relative to *hmr-1*, *hmp-1* and *hmp-2*. Taken together with the localization results, the most probable explanation is that VAB-9 activity depends on adherens junction proteins and functions downstream of HMR-1, either downstream of or parallel to HMP-1 and HMP-2.

Most mature vertebrate and invertebrate columnar epithelia are characterized by distinct apical junctional structures, and the relative positioning of apical protein complexes seems to be evolutionarily conserved[14]. Despite this conservation, only a single discernable electron-dense structure exists in the *C. elegans* epidermis[18]. DLG-1 is essential for development of this electron-dense structure, as *dlg-1* epithelia typically lack any electron-dense material[9,12]. Conversely, our data and previous studies demonstrate that neither *dlg-1* nor *ajm-1* are required for adherens junction formation or VAB-9 localization (and *vice versa*)[7,9,11–13]. These findings suggest that in *C. elegans*, the adherens junction proteins and VAB-9 are insufficient to generate electron-dense material and that they most probably localize outside the electron-dense region. As the DLG-1/AJM-1 region is localized to a similar position as the *Drosophila* septate junction and may regulate an epithelial barrier function, one possibility is that these proteins comprise part of a similar junction in *C. elegans*[9,11–13]. Our results suggest that VAB-9 functions downstream of adherens junction protein function and are consistent with a role for VAB-9 either as a direct downstream effector of adherens junction proteins or as a component of an independent junctional complex that requires the adherens junction complex for its localization. VAB-9 is similar to BCMP1, a member of a group of four-pass transmembrane proteins distantly related to the PMP22/EMP/Claudin family, which mediate homotypic cell adhesion and regulate paracellular permeability. One simple model is that the cadherin–catenin complex controls VAB-9 localization and VAB-9 then regulates the attachment and organization of a pool of circumferential F-actin at the cell junction independently of the cadherin–catenin complex. Alternatively, VAB-9 may regulate the interaction between the cadherin–catenin complex and F-actin. □

METHODS

Strains, alleles and genetics. Bristol N2 was used as the wild-type strain and handled as described[25]. Mutant alleles are listed by linkage group I (LGI): *unc-29 (e1072)*; LGV *hmp-1 (zu278)*; LGX: *ajm-1 (ok160)*.

Strains used were: JJ1136 (*unc-119* (*e2498:: Tc1*))III; *zuEx24*(*unc119*(+) *hmp-1::gfp*) (provided by J. Priess[8]). BC2991 is (*dpy-18* (*e364*)/*eT1* III; *dpy-11* (*e224*) *let-413* (*s128*) *unc-42* (*e270*)/*eT1* V)[10]. SP637 is *unc-4* (*e120*) *mnDf68*/*mnC1*. SP346 is a tetraploid strain[23]. Tetraploid animals were maintained by picking large animals from each generation.

Phenotypic analysis. *vab-9* morphological defects were scored in the entire broods of at least five *vab-9 (e2016)* animals. Egg-laying defects (Egl), dumpy (Dpy) and tail morphology defects were found in 18%, 21% and 100% ($n = 500$) of animals, respectively. The tail defect is present in all but adult males and does not seem to significantly affect mating efficiency[26]. All *vab-9* alleles display a similar range of phenotypes and are fully recessive. To determine the phenotype of *vab-9*/ *mnDf68* animals, wild-type males were crossed into *vab-9 (e1775)*, *vab-9 (e2016)* and *vab-9 (ju6)* hermaphrodites and the F1 progeny were crossed into SP637, which contains *mnDf68*, a deficiency that spans the *vab-9* locus. As expected, approximately 25% of the progeny displayed *vab-9* phenotypes: 29% for *ju6* ($n = 114$); 30% for *e1775* ($n = 120$); 26% for *e2016* ($n = 102$). All *vab-9*/ *mnDf68* animals displayed tail defects, and no lethality was observed in the F1 generation. All *vab-9*/ *mnDf68* F1 were fertile and generated 25% lethal progeny *(mnDf68*/ *mnDf68)* and a typical distribution of VAB phenotypes among *vab-9*/ *mnDf68* and *vab-9*/*vab-9* progeny.

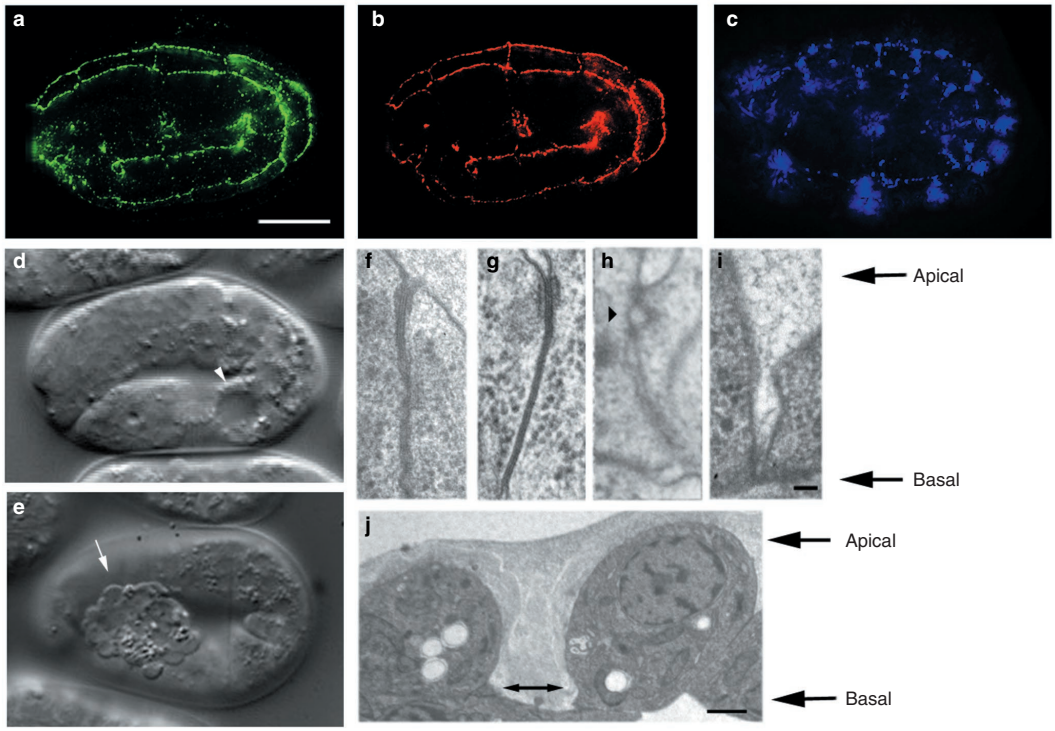

Figure 5 Interactions between *vab-9*, *ajm-1* and *dlg-1*. (**a**–**c**) Localization of VAB-9, as shown in **a**, and HMP-1, as show in **b**, is normal in *dlg-1* embryos, whereas localization of AJM-1, as shown in **c**, is disrupted. (**d**) The arrest phenotype of *dlg-1* RNAi-treated embryos, typified by the presence of a posterior vacuole (arrowhead), using DIC. (**e**) The more severe arrest phenotype of a *vab-9; dlg-1* RNAi-treated embryo. Epidermal ruptures result in loss of internal contents (arrow). (**f–i**) Lateral TEM views of apical to basal cell–cell contact regions between epidermal cells in wild-type, *vab-9, ajm-1* and *vab-9; ajm-1* animals, respectively. Arrowhead in **h** indicates characteristic separation in the apical junction of an *ajm-1* mutant. (**j**) A complete separation of lateral membranes in neighbouring epidermal cells in a *vab-9; ajm-1* embryo. Double-headed arrow indicates a gap between epidermal cells. Scale bar represents 10 μm in **a**–**e**, 100 nm in **f**–**i** and 1 μm in **j**.

***vab-9* cloning experiments.** Cosmid T22C8 rescued all *vab-9* defects completely. T22C8 contains eight predicted genes. The *vab-9* transcription unit was identified as follows. First, the rescuing region was narrowed using sub-clones of T22C8. Second, the reading frame of the predicted gene T22C8.8 was disrupted by resecting a unique *Kpn*I site into a minimal rescuing subclone, causing a frameshift before the third transmembrane domain that results in addition of four nonsense residues and the premature truncation of VAB-9. This clone does not rescue *vab-9* mutants. Third, a full-length cDNA corresponding to T22C8.8 was recovered using RT-PCR and rescued *vab-9* mutants when expressed under the control of a heat-shock promoter. Fourth, RNAi against T22C8.8, but not the other predicted genes in the minimal rescuing clone, induced *vab-9* mutant phenotypes. For each construct tested for rescue, three independent lines were generated and at least 100 array-containing animals were scored for rescue of tail, body shape and egg-laying defects. Heat-shock rescue was tested by mounting *vab-9*; *jcEx50* [pJS318, pRF4 (*rol-6d*)] on a standard 5% agar pad on a glass slide beneath a coverslip. The edges were sealed with petroleum jelly and slides were placed on a Perkin-Elmer 4800 PCR block and subjected to 10-min heat shocks at 30 °C every 2 h for a total of 10 h during late enclosure/early elongation. Embryos were recovered, allowed to develop and the presence of *vab-9* phenotypes was scored in adults.

GFP reporter proteins and strains. VAB-9–GFP was constructed by inserting the *Kpn*I fragment (containing the S65T GFP variant with three synthetic introns) from pPD119.16 into pJS229, creating pJS280. *jcIs11* was created by integrating extrachromosomal array *jcEx37 [pJS280, pRF4]*. *let-413::gfp* was constructed essentially as described[10].

Identification of lesions in *vab-9* alleles. All the introns and exons encompassing the *vab-9* locus were amplified with two primer pairs (JS21/22 and JS40/41) from single larvae using a protocol modified slightly from ref. 27. For each allele, three separate reactions were performed. The products were then cloned into pCRScript (Stratagene, La Jolla, CA) and both strands from at least two clones from each reaction were sequenced using automated fluorescent ABI BigDye sequencing.

cDNAs and northern blot analysis. A poly-dT primer with adaptors (JS81) was used to generate a first-strand cDNA from polyA+ mRNA. Primer pairs JS80 (SL1 splice leader with adaptors)/JS27 and JS25/JS80 were used to amplify the 5′and 3′ ends of the *vab-9* cDNA, respectively, using a 10:1 mix of AmpliTAQ (Amersham, Piscataway, NJ) and *Pfu* turbo (Stratagene) and the resulting PCR products were cloned into the *Srf*I site of pCRScript (Stratagene). A full-length cDNA (pJS316) was generated by subcloning the *Cla*I fragment from the 3′ construct (pJS310) into the 5′ cDNA construct (pJS313). To put *vab-9* expression under heat-shock control, the heat-shock promoter hsp16-41 (ref. 28) was amplified from pPD49.83 using JS16 and JS17 and subcloned in front of the full-length *vab-9* transcript in pJS316, resulting in pJS318. All PCR products were sequenced on both strands: no alterations in the sequence were observed (http://www. wormbase.org).

RNAi. cDNA, whole-worm genomic DNA or cosmid DNA was used as a substrate for amplification of open reading frames from genes using primers with T7 promoter sequences. Amplified T7-tagged double-stranded cDNA was a used as substrate for sense and antisense RNA production using Epicentre (Madison, WI) T7 polymerase and buffers. The mixture was then extracted with phenol/chloroform/isoamyl alcohol (25:24:1) and precipitated. RNA was resuspended in double-distilled water (DEPC-treated) to a concentration of >5 μg μl^{-1}, heated at 55 °C for 15 min and allowed to cool to room temperature. dsRNA was confirmed by gel electrophoresis, filtered through a 0.22-μm spin column (Millipore, Bedford, MA) and injected into young adult worms. Individual worms were placed on plates, and after the appearance of dead embryos, the adults were cut in half to release embryos. Embryos were either mounted for time-lapse differential interference contrast (DIC) or fluorescence

microscopy, or allowed to develop to comma and twofold stage before fixation for indirect immunofluorescence staining.

Transformations. Constructs were injected at 5–20 ng μl^{-1} along with pRF4 and unc-29+(F35D3) filler DNA at concentrations of 100 and 20 ng μl^{-1}, respectively. Extrachromosomal arrays were integrated by exposing transgenic lines to 3,000 rad γ-irradiation; integrated lines were outcrossed to a wild-type N2 strain at least four times.

Western blotting. Approximately 200 µl of mixed-stage animals were collected and insoluble fractions isolated essentially as described[29]. Fractions were separated in one dimension on a 12% denaturing polyacrylamide gel, transferred to PVDF membrane (Millipore) and blocked with 5% non-fat milk for 1 h. Filters were incubated with rabbit anti-VAB-9 antibody for 4 h at 4 °C and detected using the Immunostar kit (Biorad, Hercules, CA).

Antibodies and immunostaining. Antibody staining of embryos was performed using the freeze-cracking method, as described previously[30], with the following modifications: embryos were mounted on ring slides with two coats of poly-L-lysine (Sigma, St Louis, MO). After freeze cracking, slides were dipped into −20 °C methanol for 15 min and transferred directly to PBST (PBS containing 0.1% Tween-20) for 30 min. Slides were blocked using PBST containing 1% BSA or normal goat serum (NGS; 0.1%). Embryos were incubated with primary antibodies under coverslips overnight at 4 °C. Embryos were washed three times with PBST containing 1% BSA before addition of secondary antibodies and incubation for 2 h to overnight. Samples were then washed three times. SlowFade antifade kit (Molecular Probes, Eugene, OR) or DABCO (2.5%; Sigma) was added to the mount and a coverslip was placed over the embryos. Images were captured using a Bio-Rad MRC1024 confocal microscope (Hemel Hemstead, UK) or a DeltaVision deconvolution microscope (Applied Precision, Issaquah, WA) and projected images were created using software provided by Biorad, or using 4D macros within NIH Image[24]. Affinity purified anti-VAB-9 antibodies were raised against a C-terminal peptide created by QCB Inc. (Hopkinton, MA). Purified antibodies were used at 1:400 for immunostaining and 1:1000 for western blotting. The following additional primary antibodies were used at the dilutions indicated: MH27 at 1:1500 (a gift from M. Hresko and R. Waterston), anti-DLG-1 at 1:3000 (a gift from V. Budnik), chicken anti-PAR-3 at 1:10 (a gift from K. Kemphues), anti-UNC-70 (βG-spectrin) at 1:500 (a gift from V. Bennett). HMP-1 monoclonal (1:100), HMR-1 polyclonal (1:10) and HMP-2 polyclonal (1:100) were gifts from J. Priess and B. Leung. Phalloidin staining was performed as previously described[7].

Electron microscopy. TEM was performed as previously described[13].

Accession Numbers. VAB-9 (AY275709), *Drosophila* DVAB-9 (AAF56054) and canine BCMP1 (AJ43320).

Note: Supplementary Information is available on the Nature Cell Biology website.

ACKNOWLEDGEMENTS

The authors wish to thank J. Priess and members of the Priess lab for providing lab space, research materials and intellectual input. We specifically thank J. Priess for suggesting the use of tetraploid strain SP346 to obtain larger embryos. We thank members of the Hardin lab, M. Labouesse, L. Bruggeman, D. Sonneborn and Joe for helpful discussions. We thank J. White and W. Mohler for assistance with MPLSM, D. Hall for advice with TEM, A. Chisholm for the *vab-9 (ju6)* strain, P. Heid for cosmid pools, and A. Fire for GFP and heat-shock vectors. Some of the nematode strains used in this study were provided by the *Caenorhabditis* Genetics Centre, which is funded by the NIH National Centre for Research Resources (NCRR). The Nematode Expression Database (http://nematode.lab.nig.ac.jp/) and some cDNA clones were provided courtesy of the laboratory of Y. Kohara at the National Institute of Genetics, Japan. This work was supported by NIH grant GM58038 (J.D.H.). J.S.S. was a Helen Hay Whitney fellow. Some funds were provided by the Gamete and Embryo Training Grant from the University of Wisconsin. The Bio-Rad MRC 1024 confocal microscope at the University of Wisconsin is supported by National Science Foundation grant 9724515.

COMPETING FINANCIAL INTERESTS

The authors declare that they have no competing financial interests.

Received 6 December 2002; Accepted 30 May 2003;
Published online: 22 June 2003; DOI: 10.1038/ncb1002.

1. Notterpek, L. *et al.* Peripheral myelin protein 22 is a constituent of intercellular junctions in epithelia. *Proc. Natl Acad. Sci. USA* **98,** 14404–14409 (2001).
2. Taylor, V., Welcher, A. A., Program, A. E. & Suter, U. Epithelial membrane protein-1, peripheral myelin protein 22, and lens membrane protein 20 define a novel gene family. *J. Biol. Chem.* **270,** 28824–28833 (1995).
3. Christophe-Hobertus, C., Szpirer, C., Guyon, R. & Christophe, D. Identification of the gene encoding Brain Cell Membrane Protein I (BCMPI), a putative four-transmembrane protein distantly related to the Peripheral Myelin Protein 22/Epithelial Membrane Proteins and the Claudins. *BMC Genomics* **2,** 3 (2001).
4. Tsukita, S., Furuse, M. & Itoh, M. Multifunctional strands in tight junctions. *Nature Rev. Mol. Cell Biol.* **2,** 285–293 (2001).
5. Farquhar, M. G. & Palade, G. E. Junctional complexes in various epithelia. *J. Cell Biol.* **17,** 375–412 (1963).
6. Yeaman, C., Grindstaff, K., Hansen, M. & Nelson, W. New perspectives on mechanisms involved in generating epithelial cell polarity. *Physiol. Rev.* **79,** 73–98 (1999).
7. Costa, M. *et al.* A putative catenin–cadherin system mediates morphogenesis of the *Caenorhabditis elegans* embryo. *J. Cell Biol.* **141,** 297–308 (1998).
8. Raich, W. B., Agbunag, C. & Hardin, J. Rapid epithelial-sheet sealing in the *Caenorhabditis elegans* embryo requires cadherin-dependent filopodial priming. *Curr. Biol.* **9,** 1139–1146 (1999).
9. McMahon, L., Legouis, R., Vonesch, J. L. & Labouesse, M. Assembly of *C. elegans* apical junctions involves positioning and compaction by LET-413 and protein aggregation by the MAGUK protein DLG-1. *J. Cell Sci.* **114,** 2265–2277 (2001).
10. Legouis, R. *et al.* LET-413 is a basolateral protein required for the assembly of adherens junctions in *Caenorhabditis elegans*. *Nature Cell Biol.* **2,** 415–422 (2000).
11. Bossinger, O., Klebes, A., Segbert, C., Theres, C. & Knust, E. Zonula adherens formation in *Caenorhabditis elegans* requires dlg-1, the homologue of the *Drosophila* gene *discs large*. *Dev. Biol.* **230,** 29–42 (2001).
12. Firestein, B. L. & Rongo, C. DLG-1 is a MAGUK similar to SAP97 and is required for adherens junction formation. *Mol. Biol. Cell* **12,** 3465–3475 (2001).
13. Koppen, M. *et al.* Cooperative regulation of AJM-1 controls junctional integrity in *Caenorhabditis elegans* epithelia. *Nature Cell Biol.* **3,** 983–991 (2001).
14. Knust, E. & Bossinger, O. Composition and formation of intercellular junctions in epithelial cells. *Science* **298,** 1955–1959 (2002).
15. Baumgartner, S. *et al.* A *Drosophila* neurexin is required for septate junction and blood–nerve barrier formation and function. *Cell* **87,** 1059–1068 (1996).
16. Lamb, R. S., Ward, R. E., Schweizer, L. & Fehon, R. G. *Drosophila* coracle, a member of the protein 4.1 superfamily, has essential functions in the septate junction and developmental functions in embryonic and adult epithelial cells. *Mol. Biol. Cell* **9,** 3505–3519 (1998).
17. Mohler, W. A., Simske, J. S., Williams-Masson, E. M., Hardin, J. D. & White, J. G. Dynamics and ultrastructure of developmental cell fusions in the *Caenorhabditis elegans* hypodermis. *Curr. Biol.* **8,** 1087–1090 (1998).
18. Priess, J. R. & Hirsh, D. I. *Caenorhabditis elegans* morphogenesis: the role of the cytoskeleton in elongation of the embryo. *Dev. Biol.* **117,** 156–173 (1986).
19. Furuse, M., Fujita, K., Hiiragi, T., Fujimoto, K. & Tsukita, S. Claudin-1 and -2: novel integral membrane proteins localizing at tight junctions with no sequence similarity to occludin. *J. Cell Biol.* **141,** 1539–1550 (1998).
20. Furuse, M., Sasaki, H., Fujimoto, K. & Tsukita, S. A single gene product, claudin-1 or *-2*, reconstitutes tight junction strands and recruits occludin in fibroblasts. *J. Cell Biol.* **143,** 391–401 (1998).
21. Hresko, M. C., Williams, B. D. & Waterston, R. H. Assembly of body wall muscle and muscle cell attachment structures in *Caenorhabditis elegans*. *J. Cell Biol.* **124,** 491–506 (1994).
22. Karabinos, A., Schmidt, H., Harborth, J., Schnabel, R. & Weber, K. Essential roles for four cytoplasmic intermediate filament proteins in *Caenorhabditis elegans* development. *Proc. Natl Acad. Sci. USA* **98,** 7863–7868 (2001).
23. Herman, R. & Horvitz, H. in *Nematodes as Biological Models, Volume 1: Behavioral and Developmental Models.* (ed. Zuckerman, B.) 227–262 (Academic Press, New York, 1980).
24. Mohler, W. A. & White, J. G. Stereo-4-D reconstruction and animation from living fluorescent specimens. *Biotechniques* **24,** 1006–1010**,** 1012 (1998).
25. Brenner, S. The genetics of *Caenorhabditis elegans*. *Genetics* **77,** 71–94 (1974).
26. Hodgkin, J. Male phenotypes and mating efficiency in *C. elegans*. *Genetics* **103,** 43–64 (1983).
27. Williams, B. D., Schrank, B., Huynh, C., Shownkeen, R. & Waterston, R. H. A genetic mapping system in *Caenorhabditis elegans* based on polymorphic sequence-tagged sites. *Genetics* **131,** 609–624 (1992).
28. Stringham, E. G., Dixon, D. K., Jones, D. & Candido, E. P. Temporal and spatial expression patterns of the small heat shock (*hsp16*) genes in transgenic *Caenorhabditis elegans*. *Mol. Biol. Cell* **3,** 221–233 (1992).
29. Wang, X. *et al.* Multiple ephrins control cell organization in *C. elegans* using kinase-dependent and -independent functions of the VAB-1 Eph receptor. *Mol. Cell* **4,** 903–913 (1999).
30. Williams-Masson, E. M., Malik, A. N. & Hardin, J. An actin-mediated two-step mechanism is required for ventral enclosure of the *C. elegans* hypodermis. *Development* **124,** 2889–2901 (1997).
31. Moorthy, S., Chen, L. & Bennett, V. *Caenorhabditis elegans* β-G spectrin is dispensable for establishment of epithelial polarity, but essential for muscular and neuronal function. *J. Cell Biol.* **149,** 915–930 (2000).
32. Bilder, D. & Perrimon, N. Localization of apical epithelial determinants by the basolateral PDZ protein Scribble. *Nature* **403,** 676–680 (2000).

Epithelial polarity and integrity in *C. elegans* are generally regulated by LET-413, a basolateral LAP1 protein similar to *Drosophila* Scribble [10,32]. LET-413 is required for the localization of a number of apical proteins, participates with DLG-1 in the localization of AJM-1, but is seemingly less important for the apical localization of adherens junction proteins [9,10,13]. We determined VAB-9 localization relative to HMP-1 and AJM-1 in *let-413* mutants and *let-413; dlg-1 (RNAi)* animals and found that the apical localization of VAB-9 and HMP-1 in these embryos persists while AJM-1 protein is mislocalized within the lateral membrane. Both VAB-9 and HMP-1 also mislocalize to the most basolateral position within the lateral membrane, forming an additional discrete ring about the periphery of the cell at this position (supplemental Fig.1).

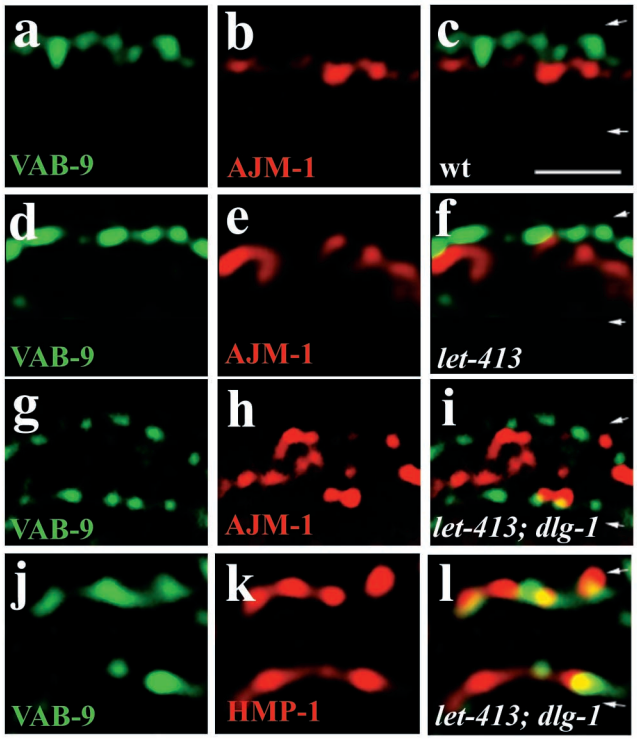

ig. S1 Localization of VAB-9, AJM-1, and HMP-1 in projected images of the lateral cell membrane between lateral seam and dorsal epidermal cells of wild-type, *let-413* and *let-413; dlg-1 (RNAi)* animals. Shown are wild-type (**a-c**), *let-413* (**d-f**), and *let-413; dlg-1 (RNAi)* (**g-l**) animals. VAB-9 immunostaining is shown in the first column (**a, d, g,** and **j**). AJM-1 immunostaining is shown in **b, c, e, f, h,** and **i**. HMP-1 immunostaining is shown in **k** and **l**. Merged images of the first two columns are shown in the right hand column. In *let-413* and *let-413; dlg-1 (RNAi)* animals, VAB-9 and HMP-1 expression is confined to the apical and basal margin, while in *let-413; dlg-1 (RNAi)* animals AJM-1 is mislocalized along the entire lateral membrane (**h, i**). Small arrows indicate the apical (top) and basal (bottom) margins of the lateral membrane, determined by co-staining with β-G-spectrin (not shown). Bar = 2 μm.